Molecular tagging velocimetry and thermometry and its application to the wake of a heated circular cylinder

Hui Hu[1] and Manoochehr M Koochesfahani[2]

[1] Department of Aerospace Engineering, Iowa State University, Ames, IA 50011, USA
[2] Department of Mechanical Engineering, Michigan State University, East Lansing, MI 48824, USA

E-mail: huhui@iastate.edu and koochesf@egr.msu.edu

Abstract
We report improvements to the molecular tagging velocimetry and
thermometry (MTV&T) technique for the simultaneous measurement of
velocity and temperature fields in fluid flows. A phosphorescent molecule,
which can be turned into a long lifetime tracer upon excitation by photons of
appropriate wavelength, is used as a tracer for both velocity and temperature
measurements. A pulsed laser is used to 'tag' the regions of interest, and
those tagged regions are imaged at two successive times within the lifetime
of the tracer molecules. The measured Lagrangian displacement of the
tagged molecules provides the estimate of the fluid velocity vector. The
simultaneous temperature measurement is achieved by taking advantage of
the temperature dependence of phosphorescence lifetime, which is
estimated from the intensity ratio of the tagged molecules in the two images.
In relation to the original molecular tagging thermometry work of
Thompson and Maynes (2001 *J. Fluid Eng.* **123** 293–302), the
improvements reported here are the use of lifetime imaging as a ratiometric
method to enhance the robustness and accuracy of temperature
measurements and the extension of the technique to simultaneous
whole-field planar mapping of velocity and temperature fields. Compared
with other simultaneous velocity and temperature measurement techniques
such as combined PIV-LIF (Sakakibara *et al* 1997 *Int. J. Heat Mass
Transfer* **40** 3163–76, Grissino *et al* 1999 *Proc. 3rd Int. Workshop on
Particale Image Velocimetry* (*Santa Barbara, CA, USA, 16–18 September
1999*)) and the DPIV/T technique (Park *et al* 2001 *Exp. Fluids* **30** 327–38),
this method accomplishes the same objectives but with a completely
molecular-based approach. Because of its molecular nature, issues such as
tracking of the flow by the seed particles and the thermal response of the
thermal tracer particles are eliminated. In addition, the use of a single
molecular tracer and a dual-frame CCD camera provides for a much reduced
burden on the instrumentation and experimental set-up. The implementation
and application of the new technique are demonstrated by conducting
simultaneous velocity and temperature measurements in the wake region of
a heated circular cylinder at a Richardson number of 0.36, a value large
enough for the buoyancy effects to potentially influence the flow.

(Some figures in this article are in colour only in the electronic version)

1. Introduction

Velocity and temperature are two important variables in studies of thermofluid problems. Simultaneous information on these two variables is often required to further our understanding of the fundamental mechanisms of complex thermofluid phenomena. In turbulent flows, the temperature field is determined by the molecular diffusion of heat and transport by the turbulent flow field. When one considers the Reynolds-averaged energy conservation equation, the effect of turbulent transport appears in terms of the correlation between the temperature and velocity fluctuations, i.e. turbulent heat flux $\overline{u'_j T'}$. Experimental characterization of these correlation terms is needed for the development and validation of physical models.

In order to measure the correlation between velocity and temperature fluctuations in turbulent flows, early studies were conducted using intrusive probes. Antonia *et al* (1975) and Chevray and Tutu (1978) employed a cold-wire sensor mounted on an X-wire probe to obtain simultaneous measurements of temperature and velocity in a heated jet flow. Kotsovinos (1977) used the combination of one-component laser Doppler velocimetry (LDV) and fast response thermistors to measure the velocity and temperature simultaneously in turbulent buoyant jets.

More recently, the advent of optical diagnostics such as LDV, laser-induced fluorescence (LIF) and Raman scattering techniques has presented new opportunities for the non-intrusive simultaneous measurements of velocity and temperature in fluid flows. By combining LDV and vibrational Raman scattering, Dibble *et al* (1984) measured the velocity and temperature in turbulent flames. Taking advantage of the temperature dependence of fluorescence emission, a combined LIF and LDV technique was used by Lemoine *et al* (1999) to conduct temperature and velocity measurements at the points of interest in a turbulent heated jet. These investigations, however, involved single-point measurements.

Whole-field diagnostic techniques such as particle image velocimetry (PIV) and LIF have led to recent efforts in the simultaneous quantification of velocity and temperature distributions over a plane. A combination of PIV and LIF has been used by Sakakibara *et al* (1997), Hishida and Sakakibara (2000) and Grissino *et al* (1999) to obtain simultaneous measurements of velocity and temperature fields in a study of heat transfer characteristics in turbulent flows. By using thermochromic liquid crystal (TLC) encapsulated microspheres as tracer particles, a digital particle image velocimetry/thermometry (DPIV/T) technique has also been developed (Dabiri and Gharib 1991, Park *et al* 2001) to achieve such simultaneous measurements.

Since the optical velocimetry techniques mentioned above are particle based, the potential implications associated with the use of seed particles need to be evaluated for each experiment. Some of these implications are related to flow tracking issues, such as particle size, density mismatch, etc. Even if particles track the flow perfectly, strong out-of-plane motions that may bring the particle tracers into and out of the laser sheet can affect the accuracy of the in-plane velocity measurements in PIV. If particles are used also for temperature measurement (e.g., TLC encapsulated microspheres), additional considerations are also required about the thermal response of the particle tracers. When PIV is combined with LIF, complications such as the influence of laser light absorption/scattering by the seed particles on the LIF signal need to be carefully considered. For the combined PIV/LIF technique, at least two cameras with various optical filters are required to record the particle scattering and LIF signals separately. A very careful image registration or coordinate mapping procedure is also required in order to get the quantitative spatial relation between the simultaneous velocity and temperature measurements.

In this paper, a completely molecular-based method is presented for the simultaneous whole-field mapping of velocity and temperature fields. The method is based on a molecular tagging approach that combines molecular tagging velocimetry (MTV) with molecular tagging thermometry (MTT). Because of its molecular nature, this method eliminates issues such as the tracking of the flow by the seed particles. A molecular-based approach has been previously reported for the simultaneous measurement of velocity and scalar concentration fields by combining MTV with LIF using two tracers, one for MTV and one for LIF (Koochesfahani *et al* 2000). The present work employs a single tracer for both MTV and MTT. The particular tracer used here is a water-soluble long-lived phosphorescent triplex that has found extensive use as a tracer for MTV (Koochesfahani *et al* 1996, Gendrich *et al* 1997). The use of this triplex for thermometry was first reported by Thompson and Maynes (2001) who coined the term molecular tagging thermometry (MTT). In that work, an intensity-based approach was utilized; the variation of phosphorescence intensity with temperature was used as the basis for thermometry. By taking advantage of the temperature dependence of the phosphorescence lifetime, Hu and Koochesfahani (2003) advanced MTT by developing a lifetime-based thermometry technique, a *ratiometric* approach to eliminate the effects of the temporal and spatial variations in the incident laser intensity and the non-uniformity of the dye concentration (e.g., due to bleaching).

Due to the nature of their implementation based on tagging molecules along single lines, however, both Thompson and Maynes (2001) and Hu and Koochesfahani (2003) were limited to combined thermometry and only one-component velocimetry in unidirectional flows. In this work, the lifetime-based ratiometric approach of Hu and Koochesfahani (2003) is extended for simultaneous whole-field planar mapping of velocity and temperature fields in a general flow field. A laser is used to 'tag' the molecules in the regions of interest;
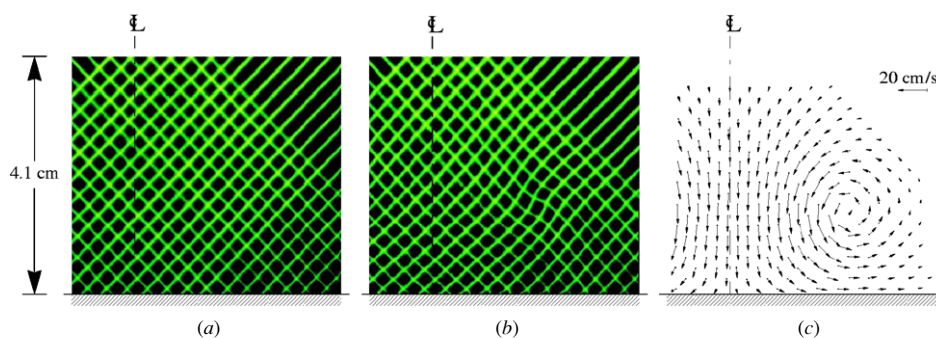
Figure 1. Typical MTV image pairs and the resultant two-component velocity field (Gendrich *et al* 1997). The flow shown is from a vortex ring impacting on a flat wall at normal incidence. The axis of symmetry is indicated by the dashed lines: (*a*) The grid imaged 1 μs after the laser pulse. (*b*) The same grid imaged 8 ms later. (*c*) The velocity field derived from (*a*) and (*b*).

the displacement of the tagged regions provides the velocity information and the phosphorescence intensity decay within those regions is used to determine the temperature. In the following sections, a brief general overview of MTV is given along with more details of lifetime-based MTT and the related properties of the phosphorescent tracer used. A demonstration of the application of this molecular-based approach is provided by carrying out simultaneous measurements of the velocity and temperature fields in the wake of a heated cylinder.

2. Molecular tagging velocimetry (MTV)

MTV is a whole-field optical technique which relies on molecules that can be turned into long lifetime tracers upon excitation by photons of appropriate wavelength. Typically, a pulsed laser is used to 'tag' the regions of interest, and those tagged regions are interrogated at two successive times within the lifetime of the tracer. The measured Lagrangian displacement of the tagged molecules provides the estimate of the velocity vector. The technique can be thought of as essentially a *molecular* counterpart of PIV and can offer advantages in situations where the use of seed particles is either not desirable, difficult, or may lead to complications. Figure 1 illustrates one implementation of the technique where the particular tracer used is a water-soluble phosphorescent supramolecule. A planar grid of intersecting laser beams, formed from a pulsed excimer laser (20 ns pulse, 308 nm wavelength), turns on the luminescence of the supramolecules that are premixed in a water flow of a vortex ring approaching a solid wall at normal incidence (Gendrich *et al* 1997). The displacement of the tagged regions is determined, in this case, using a direct spatial correlation method. The conventional planar imaging shown in figure 1 provides information on two components of the velocity vector, the projection onto the viewed plane. Stereo imaging can produce the complete three components of the velocity vector (Bohl *et al* 2001). Various advances in this measurement technique in terms of available molecular tracers, methods of tagging, detection/imaging and data processing can be found in several review articles (Falco and Nocera 1993, Koochesfahani *et al* 1996, Koochesfahani 1999, Lempert and Harris 2000), in addition to a special issue of *Measurement Science and Technology* on this topic (Koochesfahani 2000).

The work described here takes advantage of a phosphorescent supramolecule as a common molecular tracer

for both velocimetry and thermometry. It has been shown that water-soluble supramolecular complexes may be designed to exhibit long-lived phosphorescence, which is not quenched by O_2, upon mixing a lumophore, an appropriate alcohol, and cyclodextrin (Ponce *et al* 1993, Mortellaro and Nocera 1996, Hartmann *et al* 1996). The original design used in MTV (Koochesfahani *et al* 1996, Gendrich *et al* 1997) is 1-BrNp·Gβ-CD·ROH, a triplex formed by mixing the lumophore (1-BrNp), certain alcohols (indicated collectively by ROH), and an aqueous solution of glucosyl-β-cyclodextrin (Gβ-CD). The resulting long-lived green phosphorescence has a typical lifetime of up to several milliseconds. The current work utilizes the laser-induced phosphorescence of a slightly different triplex, 1-BrNp·Mβ-CD·ROH. In this triplex, the original glucose sugar subunits that are hanging off the rim of the cyclodextrin for increased solubility (i.e., glucosyl-β-cyclodextrin, Gβ-CD) have been replaced by maltose (i.e., maltosyl-β-cyclodextrin, Mβ-CD). The measured properties of both glucose- and maltose-based triplexes are quite similar and the two can be used interchangeably. The dependence of the phosphorescence lifetime on temperature, the property that is used for thermometry, will be discussed in section 3.

Tagging the molecular tracers along single or multiple parallel lines is perhaps the simplest method of tagging and has been utilized in a large fraction of studies to date. It is clear that line tagging allows the measurement of only one component of velocity that is normal to the tagged line. In addition, the estimate of this velocity component has an inherent error associated with it, which is connected with the ambiguity in the unique determination of the displacements of various portions of a (continuous) tagged line. This ambiguity can also cause significant errors in the temperature inferred from MTT in three-dimensional flows with non-uniform temperature field. In order to unambiguously measure two components of the velocity in a plane, the luminescence intensity field from a tagged region must have spatial gradients in two, preferably orthogonal, directions. For single-point velocimetry, this is easily achieved using a pair of crossing laser beams; a grid of intersecting laser lines allows multi-point velocity measurements as shown in figure 1. As already mentioned, stereo imaging would allow the recovery of the third, out-of-plane, velocity component as well.

In the original work of Gendrich *et al* (1997), for each laser pulse the MTV image pairs were acquired by a pair of aligned image detectors viewing the same region in the flow.

In the current work, the two detectors are replaced by a single intensified CCD camera (PCO DiCam-Pro) operating in the dual-frame mode, which allows the acquisition of two images of the tagged regions with a programmable time delay between them. The displacement of the tagged regions is determined by a direct digital spatial correlation technique. The details of this approach and its performance are described in Gendrich and Koochesfahani (1996). A small window, referred to as the source window, is selected from a tagged region in the earlier image, and it is spatially correlated with a larger roam window in the second image. A well-defined correlation peak occurs at the location corresponding to the displacement of the tagged region by the flow; the displacement peak is located to sub-pixel accuracy using a multi-dimensional polynomial fit. According to Gendrich and Koochesfahani (1996), the accuracy in measuring the displacement of the tagged regions depends on the signal/noise ratio of the images acquired; it can be typically determined with a 95% confidence limit of ±0.1 sub-pixel accuracy (i.e., 95% of the displacement measurements are accurate to better than 0.1 pixel). This corresponds to an rms accuracy of ±0.05 pixel, assuming a Gaussian distribution for error. For high values of image signal/noise ratio, the 95% confidence level can be as low as 0.015 pixel (0.0075 pixel rms). An example of the application of this procedure is provided in figure 1; the velocity vectors shown in this figure are 'raw' and have not been filtered or smoothed.

For velocity measurement, MTV utilizes the information about the spatial distribution of the photoluminescence of the tagged molecules within a region to determine the displacement and, therefore, the spatially averaged velocity of a tagged region. As described in the following section, monitoring the phosphorescence intensity decay rate (i.e., emission lifetime) within the tagged regions provides information on the spatially averaged temperature within those regions simultaneous with velocity information.

3. Molecular tagging thermometry (MTT)

Fluorescence and phosphorescence are molecular photoluminescence phenomena and their general properties can be found in texts on photochemistry (e.g., Turro 1978, Ferraudi 1988). Fluorescence refers to the radiative process when a molecule transitions from a singlet excited state to its singlet ground state. Since singlet–singlet transitions are quantum mechanically allowed, they occur with a high probability, making fluorscence short lived with short emission lifetimes on the order of nanoseconds. Phosphorescence, on the other hand, is a radiative process when a molecule transitions from a triplet excited state to its singlet ground state. Because such transitions are quantum mechanically forbidden, phosphorescence is long lived with emission lifetimes that may approach microseconds or even minutes. For some molecules, the photoluminescence (either fluorescence or phosphorescence) emission intensity is temperature dependent, allowing the measurement of the emission intensity of tracer molecules to be used to quantify the temperature field in a fluid flow.

The laser-induced fluorescence (LIF) technique has been widely used for fluid flow temperature measurement in recent

years. Since the fluorescence emission has a very short lifetime of order nanoseconds, molecular tagging velocimetry based on direct fluorescence is practical only for extremely fast flow velocities. Furthermore, because of the short lifetime, LIF methods typically rely on the information obtained from the 'intensity axis' of the emission process, i.e. the fluorescence intensity is used to infer the temperature. The artefacts caused by the variations in the incident laser intensity distribution are eliminated using *ratiometric* LIF techniques such as the two-dye approach (Coppeta and Rogers 1998, Sakakibara and Adrian 1999) and the single-dye two-emission-band method (Lavielle *et al* 2001). For these *ratiometric* LIF techniques, two cameras with various optical filters are required, along with a very careful image registration or coordinate mapping procedure in order to get the quantitative spatial relation between the two images. In addition, other complications also need to be carefully considered, such as the spectral conflicts and photobleaching behaviour of the two dyes in the two-dye approach (Coppeta and Rogers 1998). In the single-dye two-emission-band method, the LIF signal reduction caused by the integration of emission over a narrow spectral band necessitates special attention to issues such as signal-to-noise ratio and the choices of the image recording system and optical filters (Lavielle *et al* 2001).

Laser-induced phosphorescence has not been used as commonly as LIF for flow diagnostics in liquids because long-lived excited states suffer from O_2 quenching and, as a result, suitable molecular complexes, such as the phosphorescent triplex used here, have not been available for aqueous flows until recently. Use of phosphorescent tracers can offer certain advantages for imaging in fluid flows since the relatively long lifetime of phosphorescence allows one to take advantage of the 'time axis' in the emission process. One such advantage is the ability to perform molecular tagging velocimetry, as already described in section 2. Another is ratiometric thermometry simultaneous with velocimetry, based on the temperature dependence of phosphorescence lifetime, which is described in the following sections. Finally, two additional features inherent in phosphorescence imaging are worth noting (see Hu *et al* 2005). Recording the phosphorescence emission with a slight time delay after the excitation laser pulse can effectively eliminate the artefacts (i.e., scattering, reflection) caused by the intense excitation source. Eliminating such artefacts can be more challenging in LIF studies. Furthermore, the Stokes shift (i.e., shift in wavelength towards red) between the absorption and emission spectra is typically much larger for phosphorescence compared to fluorescence, providing yet another means to optically filter out potential contamination of the emission signal by the excitation source.

3.1. Technique basis

According to quantum theory (Pringsheim 1949), the intensity decay of a first-order photoluminescence process (either fluorescence or phosphorescence) from a single excited state can be expressed in the form

$$I_{em} = I_0 \, e^{-t/\tau}, \tag{1}$$

where the lifetime τ refers to the time when the intensity drops to 37% (i.e., $1/e$) of the initial intensity I_0. For an excited state,

the deactivation processes may involve both radiative and non-radiative pathways and the lifetime of the photoluminescence process, τ, is determined by the sum of all the deactivation rates, i.e. $\tau^{-1} = k_r + k_{nr}$, where k_r and k_{nr} are the radiative and non-radiative rate constants, respectively. According to photoluminescence kinetics, the non-radiative rate constant is, in general, temperature dependent (Ferraudi 1988), and the resulting temperature dependence of the phosphorescence lifetime is the basis of the present technique for temperature measurement. The non-radiative rate constant k_{nr} encompasses all decay pathways that do not lead to photon emission and can include processes such as collisional deactivation, internal conversion, intersystem crossing and back intersystem crossing. Among these, collisional deactivation is generally temperature dependent and the back intersystem crossing becomes temperature dependent with the introduction of a rate constant with a non-zero activation energy.

The idea of temperature measurement by measuring the phosphorescence lifetime was also suggested by Brewster *et al* (2001) in a single-point feasibility study using oscilloscope-based instrumentation and a water-soluble phosphorescent compound. The compound utilized, however, had a relatively short lifetime of 100 μs (at room temperature), nearly 50 times smaller than that reported herein, which makes it suitable for simultaneous velocity and temperature measurements only for very high-speed water flows. The work described in the present paper represents, to our knowledge, the first whole-field temperature field measurements over a plane conducted in an aqueous flow based on the direct imaging of phosphorescence lifetime with a conventional image detecting CCD camera.

Consider capturing the phosphorescence emission by a gated CCD detector where the integration starts at a delay time t_0 after the laser excitation pulse with an integration (or gate) period of δt. The phosphorescence signal S collected by the detector is then given by

$$S = \int_{t_0}^{t_0+\delta t} I_0 \, e^{-t/\tau} \, dt = I_0 \tau (1 - e^{-\delta t/\tau}) \, e^{-t_0/\tau}. \quad (2)$$

In this expression, the initial intensity I_0 contains all the information about the incident laser intensity, the dye concentration, its absorption coefficient and the phosphorescence quantum yield (Hu and Koochesfahani 2003, Hu *et al* 2005). Thus, the phosphorescence signal may, in principle, be used to measure the temperature if the incident laser intensity and the concentration of the phosphorescent dye remain constant (or are known) in the measurement region. This is the approach taken in the original work of Thompson and Maynes (2001), where they quantified the temperature using the phosphorescence intensity of 1-BrNp·Gβ-CD·ROH acquired with a short fixed time delay (8 μs) after the laser pulse. Furthermore, the fact that the phosphorescence signal is a function of delay time t_0, which is a controllable parameter, can be utilized to significantly increase the sensitivity of temperature measurements (Hu *et al* 2005).

Now consider imaging the phosphorescence signal at two successive times, as in MTV measurements described earlier; see the schematic in figure 2. The first image is detected at the time $t = t_0$ after laser excitation for a gate period δt to accumulate the phosphorescence intensity S_1, while the second
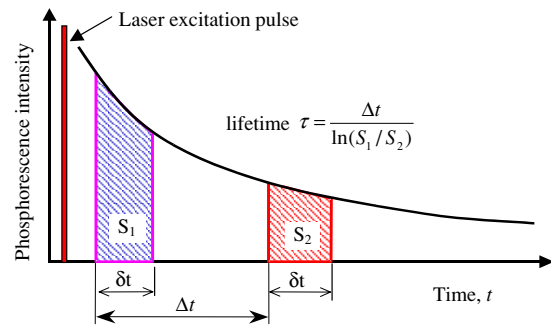
Figure 2. Timing chart for phosphorescence image pair acquisition and calculation of lifetime.

image is detected at the time $t = t_0 + \Delta t$ for the same gate period to accumulate the phosphorescence intensity S_2. It is easily shown, using equation (2), that the ratio of these two phosphorescence signals is given by

$$\frac{S_2}{S_1} = e^{-\Delta t/\tau}. \quad (3)$$

In other words, the intensity ratio of the two successive phosphorescence images is only a function of the phosphorescence lifetime τ and the time delay Δt between the images, which is a controllable parameter. This ratiometric approach eliminates the variations in the initial intensity and, along with it, any temporal and spatial variations in the incident laser intensity and non-uniformity of the dye concentration (e.g., due to bleaching). The phosphorescence lifetime can be calculated according to

$$\tau = \frac{\Delta t}{\ln(S_1/S_2)}, \quad (4)$$

resulting in the distribution of the phosphorescence lifetime over a two-dimensional domain, and the temperature distribution in the flow as long as the temperature dependence of phosphorescence lifetime is known. The next section describes the calibration of the phosphorescence lifetime variation with temperature for the phosphorescent triplex used here.

3.2. Calibration procedure for temperature dependence of phosphorescence lifetime

The current work is based on the laser-induced phosphorescence of the water-soluble triplex 1-BrNp·Mβ-CD·ROH. The alcohol (ROH) used here was cyclohexanol. The chemical composition of the triplex affects the emission intensity and lifetime. The molar concentrations of the three constituents of the triplex were according to those recommended by Gendrich *et al* (1997), i.e. 2×10^{-4} M for Mβ-CD, approximately 1×10^{-5} M for 1-BrNp (a saturated solution) and 0.06 M for the alcohol. The same composition was used for the calibration and the actual experiments described in section 4.

Figure 3 shows the schematic set-up of the calibration procedure employed to quantify the temperature dependence of phosphorescence lifetime. A Lambda-Physik XeCl excimer laser (wavelength $\lambda = 308$ nm, energy 50 mJ/pulse, pulse width 20 ns) with appropriate optics was used to generate a laser sheet (thickness about 1 mm) to illuminate a cube-shaped
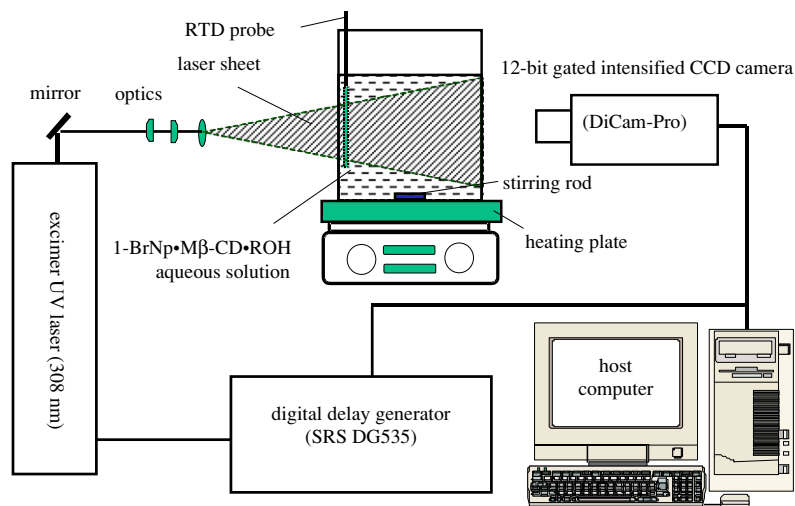
Figure 3. Schematic set-up for temperature calibration procedure.
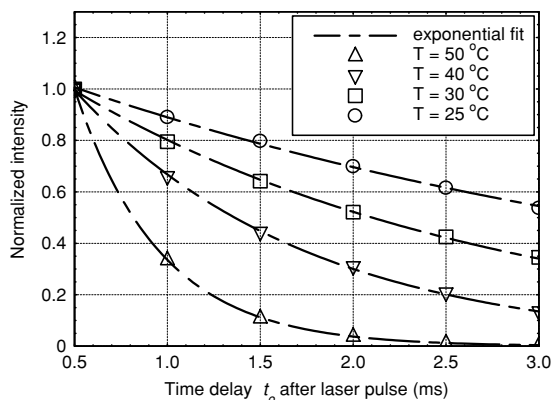

Figure 4. Phosphorescence intensity decay curves at several temperatures.

test cell (about 3 l in volume) containing an aqueous solution of 1-BrNp·Mβ-CD·ROH complex. The apparatus was placed on a heating plate and a stirring rod was used to achieve thermal equilibrium in the test cell. An RTD probe (Hart Scientific Model 1502A, temperature accuracy ±0.01 °C) was placed in one corner of the apparatus to measure the actual temperature in the test cell. During the experiment, the temperature uniformity inside the test cell was checked and was found to be within 0.1 °C.

A 12-bit, 1280 × 1024 pixel, gated intensified CCD camera (PCO DiCam-Pro) with a fast decay phosphor (P46) was used to capture the phosphorescence emission. The laser and the camera were synchronized using a digital delay generator (SRS DG535), which controlled the delay time t_0 between the laser pulse and the start of image capture. The phosphorescence images captured by the CCD camera were subsequently transferred to a host computer for analysis. In the present study, the exposure (gate) period was set to a fixed value of $\delta t = 1$ ms.

To acquire the calibration data, the aqueous solution of 1-BrNp·Mβ-CD·ROH was first heated to a pre-determined temperature level T. After thermal equilibrium was established, the phosphorescence images were acquired as a function of time delay t_0. The process was repeated
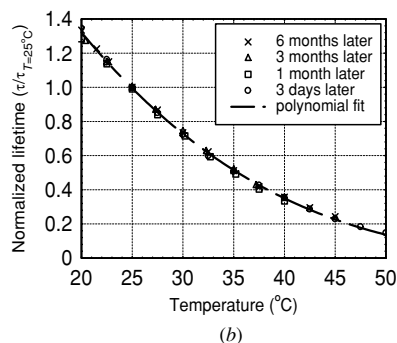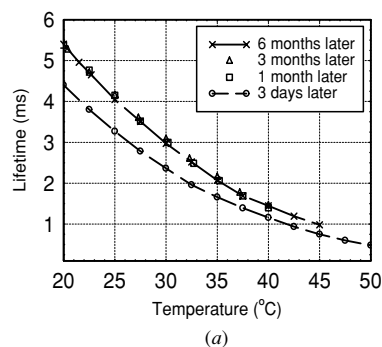

Figure 5. Variation of phosphorescence lifetime versus temperature. (*a*) The aging effect of the solution. (*b*) Normalized lifetime versus temperature.

for different solution temperatures. Figure 4 depicts the measured phosphorescence intensity decay curves at several temperatures. It can be seen that the phosphorescence intensity decay curves are very well approximated by single-exponential curves, as expected theoretically. The variation of the measured lifetime versus temperature $\tau(T)$ is shown in figure 5(*a*) at different times after the preparation of the original solution. We note that the absolute values of measured lifetime initially change slightly after the solution preparation before they finally stabilize. This 'aging' effect is believed to be connected to the solubility of the three constituents of the phosphorescent triplex and their reaching the final equilibrium state. It is found, however, that the normalized lifetime,
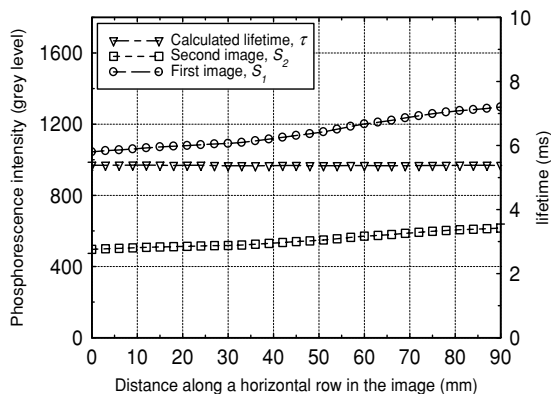
Figure 6. Intensity profiles extracted from an arbitrarily selected horizontal row in the two phosphorescence images and the derived lifetime (test cell temperature $T = 20\,°C$).

i.e. lifetime normalized by its value at a reference temperature, collapses the various lifetime curves of figure 5(*a*) onto a single 'universal' curve that is characteristic of the phosphorescent triplex used here. The normalized lifetime, using 25 °C as the reference temperature, is shown in figure 5(*b*). It is this curve that is used for the lifetime-based thermometry in this work.

It can be seen in figure 5(*b*) that the phosphorescence lifetime of 1-BrNp·Mβ-CD·ROH varies significantly with temperature. The relative temperature sensitivity of the phosphorescence lifetime ranges between 5.0% per °C at 20 °C to 20.0% per °C at 50 °C. To put these values in perspective, we note that the temperature sensitivity of the commonly used LIF dye rhodamine B is about 2.0% per °C. The calibration profiles of Thompson and Maynes (2001) indicate a temperature sensitivity of 3% per °C for their intensity-based approach with the same phosphorescent tracer used here.

In order to demonstrate the effectiveness of the present *ratiometric* technique for temperature measurement, sample intensity profiles are shown in figure 6 from the first and second phosphorescence images in the calibration test cell with the fluid temperature being maintained at a constant temperature of $T = 20$ °C. These intensity profiles were extracted from an arbitrarily selected horizontal row in the two images. It can be seen that the phosphorescence intensities of the first and second images change significantly along the beam propagation direction due to the combined effect of non-parallel beam propagation, attenuation effects and possible dye bleaching. However, the calculated phosphorescence lifetime remains constant, as expected, at a level corresponding to the test cell temperature.

4. Application to the wake of a heated cylinder

In order to demonstrate the feasibility of the technique described above, MTV&T is applied to conduct simultaneous temperature and velocity measurements in the wake of a heated cylinder. This feasibility study is similar in nature to the work of Park *et al* (2001) in connection with the development of the DPIV/T technique, except that here we consider a flow direction opposite to the gravity vector and a much higher Richardson number of 0.36 (compared to their quoted value
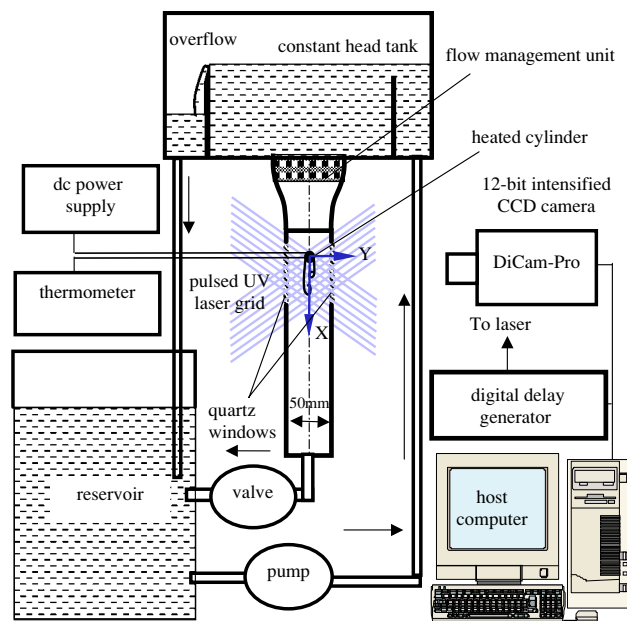
Figure 7. Experimental set-up.

of 0.01), a value large enough for the buoyancy effects to potentially influence the flow. More detailed discussion of issues affecting the measurement accuracy and resolution will be given in section 5.

4.1. Experimental set-up and flow conditions

A schematic of the experimental set-up is shown in figure 7. The test cylinder was installed horizontally in a gravity-driven vertical water channel. The dimensions of the test section were 50 mm (width) × 30 mm (height) × 200 mm (length). Two sides of the test section contained quartz windows to allow the transmission of the excimer laser UV light. The 1-BrNp·Mβ-CD·ROH phosphorescent triplex was premixed with water in a reservoir tank. A constant head tank was used to maintain a steady inflow condition during the experiment. The constant head tank was filled from the reserve tank by using an electric pump. A convergent section with honeycomb and mesh structures was used upstream of the test section to produce a uniform condition for the flow approaching the test cylinder. The velocity of the flow in the water channel was adjustable by operating the valve at the downstream end of the water channel.

A copper tube with outer diameter of $D = 4.76$ mm and inner diameter of 4.00 mm was used as the test cylinder. The cylinder was heated using a 3.1 mm diameter rod cartridge heater (Watlow Firerod) that was placed inside the copper tube. High thermal conductivity paste (OMEGATHERM 201) was pressed in to fill the gap between the rod cartridge heater and the inner wall of the copper tube. The rod cartridge heater was powered by a dc power supply (Kepco, BOP-200-2M). Two J-type thermocouples were embedded in the gap at the mid-span of the cylinder at two angular locations to provide the estimate of the cylinder temperature. The thermocouples were connected to a two-channel thermometer (Omega HH23), which had a resolution of ±0.1 °C.
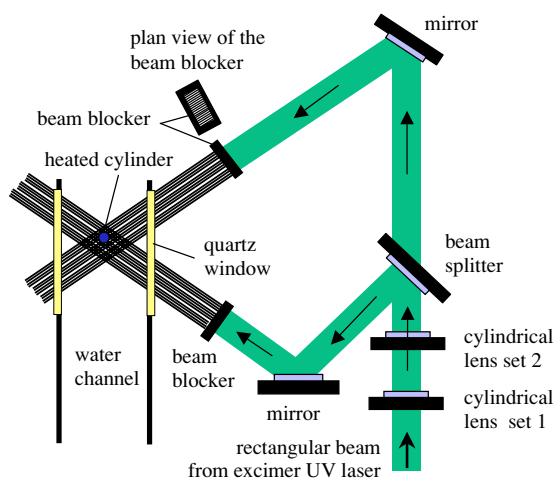
Figure 8. Schematic of optical set-up.

In order to measure two components of the velocity in the wake of the test cylinder, a grid of intersecting laser lines were used for molecular tagging. Figure 8 shows the schematic of the optical set-up, which is based on the earlier work of Gendrich *et al* (1997). The 20 ns, 150 mJ/pulse rectangular beam from an excimer UV laser (308 nm wavelength) was manipulated by a set of cylindrical optics to increase its aspect ratio. The resulting laser sheet was split by a 50:50 beam splitter; each of the two resulting sheets passed through a beam blocker to generate the grid pattern. The beam blocker was simply an aluminium plate with a series of thin slots. The camera and timing electronics arrangement for image acquisition were exactly the same as previously described for the calibration procedure, except that the camera was operated in the dual-frame mode, where two full-frame images of phosphorescence were acquired in quick succession from the same laser excitation pulse. For the present study, the first and second phosphorescence images were captured at time delays of 1 ms and 5 ms, respectively, after the laser pulse, resulting in a fixed time delay $\Delta t = 4$ ms between the two images. The integration (gate) period was 1 ms for both.

For the present study, the approach flow velocity in the water channel measured at about ten diameters upstream of the test cylinder was $U_{\text{inlet}} = 0.032$ m s^{-1} and the temperature of the incoming flow was $T_{\text{inlet}} = 23.2$ °C. The temperature of the test cylinder was maintained at $T_{\text{c}} = 56.5$ °C. Using the properties of water at the temperature of incoming flow, the flow conditions correspond to a Reynolds number $Re_D = \frac{U_{\text{inlet}}D}{\nu} = 160$, Grashof number $Gr_D = \frac{g\beta(T_{\text{c}}-T_{\text{inlet}})D^3}{\nu^2} = 9100$ and Richardson number $Ri_D = \frac{Gr_D}{Re_D^2} = 0.36$.

4.2. Measurement results

Figure 9 shows a typical pair of phosphorescence images acquired after the excitation laser pulse for the experimental conditions described above. The dark bands on the top right of the images are shadows caused by the cylinder blocking the laser beams. The 'dark regions' in the phosphorescence images downstream of the cylinder correspond to the warm fluid shedding periodically from the hot boundary layer around the heated cylinder. From the comparison of the two images, it can be seen that the dark regions become more pronounced as the time delay between the laser pulse and phosphorescence acquisition increases. This is due to the fact that the warmer fluid has a shorter phosphorescence lifetime, resulting in a larger decay in emission intensity than that in the cooler ambient fluid.

From the image pair shown in figure 9, the instantaneous velocity distribution can be derived by measuring the displacements of the tagged regions using a spatial correlation approach described briefly in section 2, with details given in Gendrich and Koochesfahani (1996). A source (or interrogation) window size of 32×32 pixels (corresponding to a region 1.12 mm $\times$ 1.12 mm in physical space) was used in the present study, along with 50% overlap between consecutive windows. Figure 10(a) shows the instantaneous velocity distribution determined from the image pair of figure 9. Each velocity vector represents an average over the source window, which dictates the spatial resolution of the measurement in this case (the maximum measured displacement of the source window by the flow was about 4 pixels, much smaller than the size of the source window). Note that velocity data are not available within the shadow regions caused by the cylinder blocking the laser light. An important aspect that needs to be emphasized is that the fixed 32×32 pixel $(0.25D \times 0.25D)$
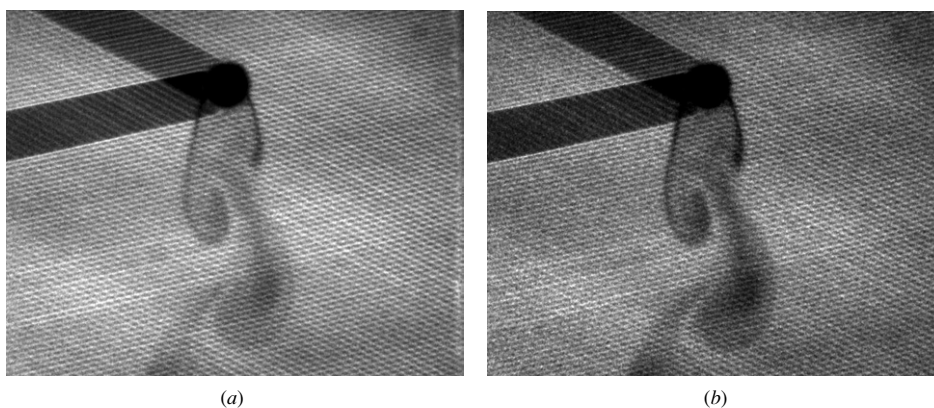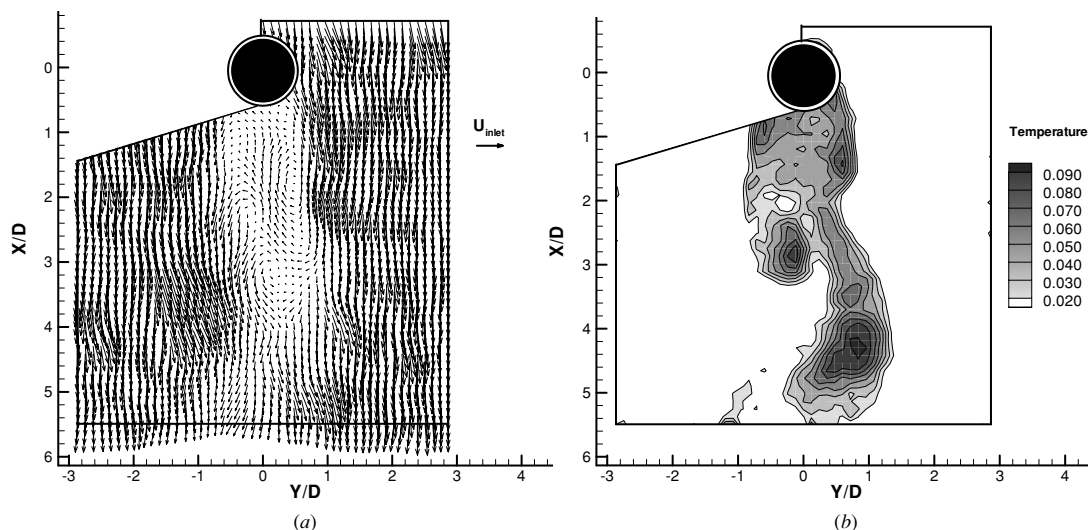

(a)

(b)

Figure 9. A typical phosphorescence image pair used for MTV&T measurements. (*a*) First image acquired 1 ms after laser pulse. (*b*) Second image acquired 5 ms after laser pulse.

Figure 10. The instantaneous velocity and temperature fields derived from the image pair in figure 9. Temperature normalization is $(T - T_{inlet})/(T_c - T_{inlet})$; the contour map starts at 0.02 with a contour spacing of 0.01. (*a*) Instantaneous velocity field. (*b*) Instantaneous temperature field.

source window used here is too large to resolve the details of the initial shear layers that separate from the cylinder. The measurements become reliable once the scales of the flow become comparable to the cylinder diameter after the shear layers roll up (beyond a downstream location $x/D > 2.5$).

The instantaneous velocity field, figure 10(*a*), shows a long re-circulation region downstream of the heated cylinder, extending to an x/D of about 3.2 in this realization, and unsteady shedding of vortex structures. These general features are similar to the case of an unheated, isothermal, cylinder. By contrast, however, the time series of the measured instantaneous velocity field indicates that the unsteady vortex structures shed periodically at a frequency of $f \approx 1.03$ Hz, corresponding to a Strouhal number $St \equiv fD/U \approx 0.15$ for the present experimental condition. This value is noticeably smaller than the Strouhal number of about 0.18 found in the literature (also confirmed in our experiments, results not shown) for an unheated cylinder at the Reynolds number of 160 in this experiment. This is believed to be a buoyancy-induced effect; a systematic study of the influence of increasing Richardson number on vortex shedding is currently under way.

The image pair in figure 9 allows the determination of the temperature distribution simultaneous with the velocity field already described. Consistent with the correlation method used for the measurement of the displacement of tagged regions, the same interrogation regions of 32 × 32 pixels in size were chosen in the first phosphorescence image to provide the average phosphorescence intensity S_1 within those regions. The molecules tagged within each region convect to a new region in the second phosphorescence image according to their Lagrangian displacement by the flow over the time delay between the two images. This displacement field is, of course, the basis of measuring the velocity field with MTV and is already available from figure 10(*a*). The mass diffusion of tagged molecules out of interrogation

windows is negligibly small (the mass diffusion length in this experiment is about 1/500 of the interrogation window size). Therefore, for each interrogation window in the first phosphorescence image, the position of the corresponding 'displaced' window in the second phosphorescence image was determined based on the already measured velocity field, and this provided the corresponding average phosphorescence intensity S_2 within each region. Note that the procedure here is a first-order method that uses a linear displacement model consistent with small Lagrangian displacements (i.e., small time delay between images) and small distortion of the tagged regions due to velocity gradients. Once the average phosphorescence intensities, S_1 and S_2, were determined for the corresponding regions in the two phosphorescence images, the phosphorescence lifetime was calculated based on equation (4), resulting in the measurement of temperature according to the lifetime-versus-temperature calibration curve in figure 5. This measurement represents an average temperature over the interrogation window. The phosphorescence intensity averaging treatment described above is helpful to improve the temperature measurement accuracy, but at the expense of reducing the spatial resolution of the measurement (see further discussion in section 5).

The simultaneous temperature field derived from the phosphorescence image pair, which is shown in figure 10(*b*), illustrates the overall temperature distribution in the wake of the heated cylinder. The alternate shedding of 'warm blobs' associated with the Karman vortices is clearly seen. Similar to velocity results, the fixed 32 × 32 pixel (0.25D × 0.25D) source window that was used is too large to resolve the details of the initial thermal shear layers that separate from the cylinder. The dark regions in figure 9 highlighting the warm boundary layers that separate from the cylinder surface suggest a value of about 0.1D for the initial thickness of these thermal shear layers. The temperatures indicated in figure 10(*b*) in those regions are, therefore, highly averaged spatially and
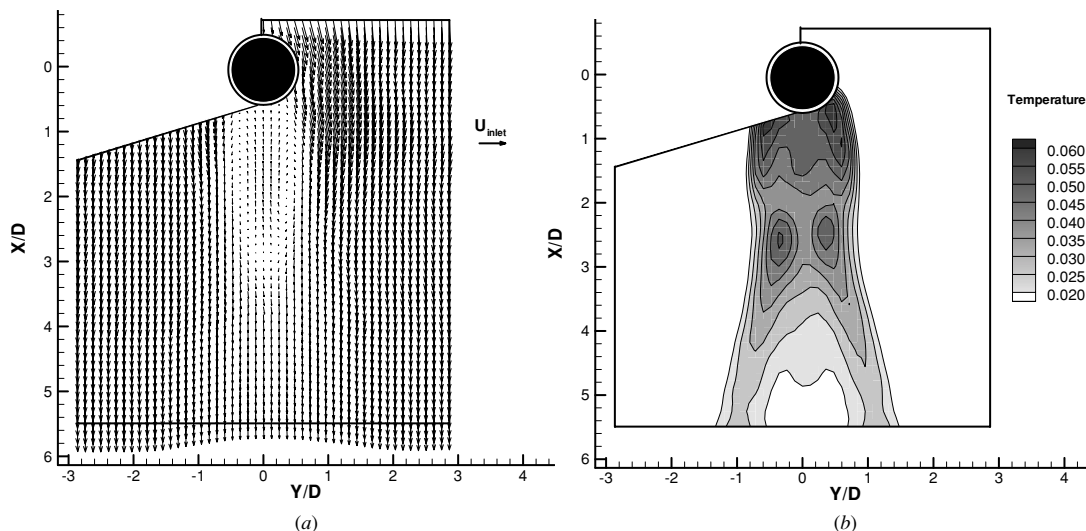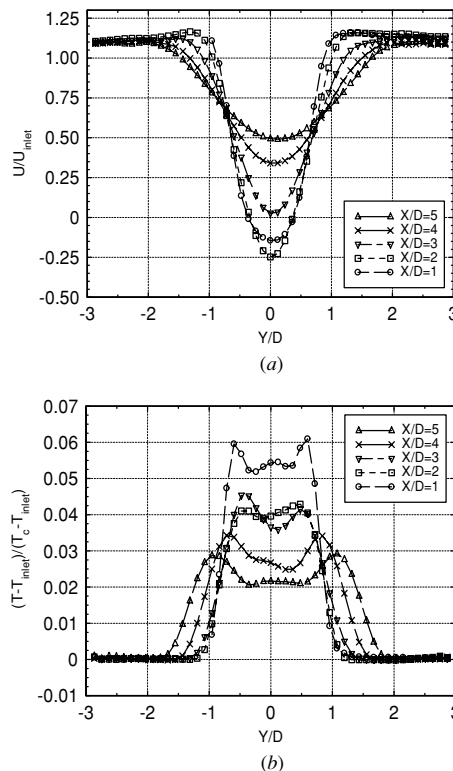
Figure 11. Mean velocity and temperature distributions. Temperature normalization is $(T - T_{inlet})/(T_c - T_{inlet})$; the contour map starts at 0.02 with a contour spacing of 0.005. (*a*) Mean velocity field. (*b*) Mean temperature field.

underestimated in magnitude. The measurements become reliable once the scales of the flow become comparable to the cylinder diameter after the shear layers roll up, after about $x/D > 2.5$. We note that the peak temperature in the centre of the warm blob ($x/D \approx 4.5$) reaches a normalized value of $(T - T_{inlet})/(T_c - T_{inlet}) \approx 0.095$, corresponding to a temperature differential of only $(T - T_{inlet}) \approx 3.1\,^{\circ}\text{C}$.

The mean velocity and temperature fields were calculated from 350 instantaneous measurements, and their overall distributions are shown in figure 11. Sample transverse profiles of the mean streamwise velocity and temperature at five downstream locations $x/D = 1, 2, 3, 4$ and 5 are also extracted from figure 11 and are given in figure 12 for a more quantitative interpretation of results. From the mean velocity results, it can be seen that the mean length of the re-circulation region in the wake behind the heated cylinder is about 2.9 cylinder diameters for the present experimental condition. The downstream evolution of the mean streamwise velocity is as expected, with a decreasing velocity deficit in the wake and an increasing width of the wake. The mean temperature distribution and the corresponding transverse profiles reveal a double-peaked temperature distribution with the two high temperature regions occurring at the two sides of the wake corresponding to the shedding paths of the 'warm blobs' revealed in the instantaneous temperature fields.

Since the velocity and temperature fields were measured simultaneously, the correlation between the velocity and temperature fluctuations can be calculated to generate the distribution of the mean turbulent heat flux $\overline{u'_j T'}$, as shown in figure 13. In interpreting this figure, it is again important to recognize the resolution difficulties in the initial regions of the wake that was mentioned earlier. We note that heat flux vectors become pronounced at about $x/D \approx 2.5$, the location where the shear layers roll up into large Karman vortices. The largest heat flux vectors are observed on the two sides of the wake corresponding to the passage of the Karman vortices.

Figure 12. Mean velocity and temperature profiles at various downstream locations. (*a*) Mean velocity profiles. (*b*) Mean temperature profiles.

5. Resolution limitations and measurement accuracy

The present MTV&T technique, like most measurement techniques, does not give information at a 'point'. Rather, it provides the spatially averaged velocity and temperature of a molecularly tagged region. Similar to PIV, the effective spatial resolution of the measurement is given by the sum of the source
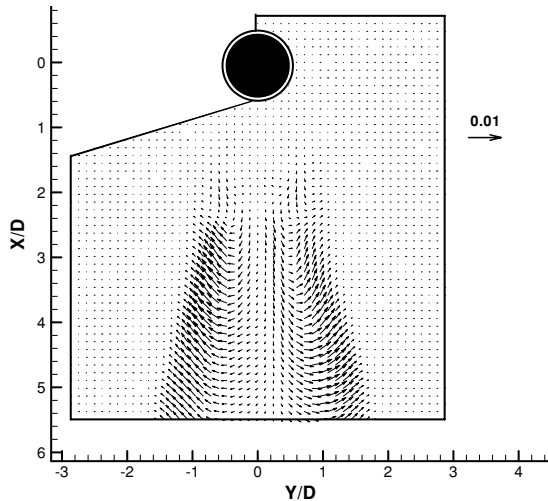
Figure 13. Spatial map of the mean turbulent heat flux; normalization: $\overline{u'_j T'}/U_{\text{inlet}}(T_c - T_{\text{inlet}})$.

window size and the measured Lagrangian displacement. In the work presented here, the spatial resolution was dominated by the source window size of 32×32 pixels (1.12 mm $\times 1.12$ mm in physical space or $0.25D \times 0.25D$). Clearly, obtaining resolved data for small scales would require tagging regions, and selecting interrogation windows, consistent with the scales to be resolved. While the best spatial resolution that can be achieved with MTV&T is set by the diffraction limitations of optics used to generate the tagging pattern and the resolution characteristics of image detection; the selection of the source (interrogation) window often involves a choice between the spatial resolution of the measurement versus the accuracy of the instantaneous measurement. This aspect will be further discussed later in this section in the context of thermometry. The temporal resolution of the present measurement methodology is set by the time delay Δt between the phosphorescence image pair, which in these experiments was 4 ms. The choice of this time delay influences the accuracy of the velocity data (larger Δt leads to larger Lagrangian displacement of tagged molecules) and the temperature estimation through equation (4); see later discussion.

The accuracy of velocity measurements using MTV depends on many parameters such as the signal-to-noise ratio in the MTV image pair, the intersection angle and width of the laser beams used for tagging, and the size of the source window used for the correlation process. These effects have been systematically studied and documented in Gendrich and Koochesfahani (1996). Based on the results of Gendrich and Koochesfahani (1996), and the present experimental conditions, the uncertainty in the measurement of the displacement of tagged regions is given by a 95% confidence limit of about ±0.2 pixel, or an rms accuracy of ±0.1 pixel, assuming a Gaussian distribution for error. Considering a maximum displacement of 4 pixels in the current measurements, the instantaneous velocity accuracy is about 2.5%.

The accuracy of temperature measurements is affected by two primary factors, the image noise in the two

phosphorescence images leading to noise in the estimated lifetime and potential inaccuracies in the identification of the region in the second phosphorescence image corresponding to the original tagged region in the first image. These issues are separately addressed below.

The accuracy in the determination of lifetime from equation (4), and the resulting accuracy in temperature measurement, is directly influenced by noise in the two phosphorescence signals S_1 and S_2. Even though a 12-bit camera is used in the present study, the actual image noise at each pixel, characterized by the standard deviation of the signal, is much higher and is in the 3% range. This noise level is connected to the CCD depth of well and the intensifier stage of the CCD. The accuracy in calculating the phosphorescence lifetime can be estimated by

$$\frac{\sigma_\tau}{\tau} = \frac{1}{\ln(S_1/S_2)}\sqrt{\left(\frac{\sigma_{S_1}}{S_1}\right)^2 + \left(\frac{\sigma_{S_2}}{S_2}\right)^2},$$

suggested by Ballew and Demas (1999), where σ_{S_1}, σ_{S_2} and σ_τ are the standard deviations of S_1, S_2 and τ, respectively. The aforementioned 3% phosphorescence signal accuracy at each pixel will, therefore, result in a lifetime measurement accuracy of about 4% and an instantaneous temperature error of 0.8 °C (using the lifetime temperature sensitivity of 5.0% per °C at 20 °C for reference). Since this error is unbiased, it can be substantially reduced by averaging over neighbouring pixels. Assuming statistical independence, the error can be reduced by the factor $1/\sqrt{N}$, where N is the number of pixels in the interrogation window. For the results given in the present study based on 32×32 pixel interrogation windows, the instantaneous measurement error due to the noise in the phosphorescence images is estimated to be less than 0.10 °C.

The MTT method described here is a Lagrangian approach. The molecular region tagged in the first image convects to a new region in the second image according to its Lagrangian displacement over the time delay between the two images. To determine the phosphorescence lifetime correctly, this new region in the second phosphorescence image needs to be identified. The effect of mass diffusion being negligible, the new region is determined solely on the basis of advection by the flow. In this work, for each interrogation window in the first phosphorescence image, the identification of its corresponding region in the second phosphorescence image was based on the Lagrangian displacement by the amount already determined by the correlation method in MTV. This is a first-order method that uses a linear displacement model consistent with small Lagrangian displacements (i.e., small time delay between images) and small distortion of the tagged regions due to velocity gradients. Higher order processing methods can, in principle, be developed to take image distortions into account. Meanwhile, two methods were used to obtain a quantitative estimate of temperature measurement error caused by distortions due to velocity gradients and the inaccuracy of the velocity measurement itself. The temperature field was computed using regions in the second phosphorescence image that were deliberately displaced an additional ±1 pixel (i.e., 25% of maximum displacement) relative to the actual location computed by MTV. This 'induced' mismatch resulted in a temperature error of about 0.1 °C for the conditions of

the present experiments. In addition, when the procedure described here was applied to the case of an unheated cylinder, for which the temperature field is uniform and constant, the measured instantaneous temperature in the freestream region was found to have an uncertainty of about 0.16 °C. In the wake region, where the effect of distortion would be more noticeable, the maximum uncertainty in temperature measurement increased to about 0.23 °C. This is the total uncertainty and accounts for all the effects discussed above.

6. Conclusions

A completely molecular-based method is presented for the simultaneous whole-field mapping of velocity and temperature fields in aqueous flows. The method uses a molecular tagging approach that combines molecular tagging velocimetry (MTV) with molecular tagging thermometry (MTT), and because of its molecular nature it eliminates issues such as the tracking of the flow by seed particles. The water-soluble phosphorescent triplex, 1-BrNp·Mβ-CD·ROH, is used as a tracer for both velocity and temperature measurements. A pulsed laser is used to 'tag' the molecules in the regions of interest; the displacement of the tagged regions provides the velocity information and the phosphorescence intensity decay within those regions is used to determine the temperature through the temperature dependence of phosphorescence lifetime. The resolution limitations and measurement uncertainties are discussed and they provide information on how to optimize these characteristics for particular flow conditions.

The implementation of the MTV&T method is demonstrated by its application to a study of the wake behind a heated cylinder at $Re = 160$. In addition to the simultaneous measurements of the instantaneous velocity and temperature fields, other mean flow quantities are measured, such as the mean velocity, temperature and velocity–temperature correlation fields. These measurements demonstrate MTV&T can be a viable tool for accurate whole-field mapping of velocity and temperature in fluid flows.

Acknowledgments

References

Antonia R A, Prubhu A and Stephenson S E 1975 Conditionally sampled measurements in a heated turbulent jet *J. Fluid Mech.* **72** 455–80

Ballew R M and Demas J N 1999 An error analysis of the rapid lifetime determination method for the evaluation of single exponential decay *Anal. Chem.* **61** 30–3

Brewster R E, Kidd M J and Schuh M D 2001 Optical thermometer based on the stability of a phosphorescent 6-bromo-2-naphthal/α-cyclodextrin$_2$ ternary complex *Chem. Commun.* 1134–5

Bohl D, Koochesfahani M and Olson B 2001 Development of stereoscopic molecular tagging velocimetry *Exp. Fluids* **30** 302–8

Chevray R and Tutu N K 1978 Intermittency and preferential transport of heat in a round jet *J. Fluid Mech.* **88** 133–60

Coppeta J and Rogers C 1998 Dual emission laser induced fluorescence for direct planar scalar behavior measurements *Exp. Fluids* **25** 1–15

Dabiri D and Gharib M 1991 Digital particle image thermometry: the method and implementation *Exp. Fluids* **11** 77–86

Dibble R W, Kollmann W and Schefer R W 1984 Conserved scalar fluxes measurement in a turbulent non-premixed flame by combined laser Doppler velocimetry and laser Raman scattering *Combust. Flame* **55** 307–21

Falco R E and Nocera D G 1993 Quantitative multipoint measurements and visualization of dense solid–liquid flows using laser induced photochemical anemometry (LIPA) *Particulate Two-Phase Flow* ed M C Rocco (Portsmouth, NH: Butterworth-Heinemann) pp 59–126

Ferraudi G J 1988 *Elements of Inorganic Photochemistry* (New York: Wiley-Interscience)

Gendrich C P and Koochesfahani M M 1996 A spatial correlation technique for estimating velocity fields using molecular tagging velocimetry (MTV) *Exp. Fluids* **22** 67–77

Gendrich C P, Koochesfahani M M and Nocera D G 1997 Molecular tagging velocimetry and other novel application of a new phosphorescent supramolecule *Exp. Fluids* **23** 361–72

Grissino A S, Hart D P and Lai W T 1999 Combined dual emission LIF and PIV to resolve temperature and velocity *Proc. 3rd Int. Workshop on Particle Image Velocimetry (Santa Barbara, CA, USA, 16–18 September 1999)*

Hartmann W K, Gray M H B, Ponce A and Nocera D G 1996 Substrate induced phosphorescence from cyclodextrin · lumophore host–guest complex *Inorg. Chim. Acta* **243** 239–48

Hishida K and Sakakibara J 2000 Combined planar laser-induced fluorescence—particle image velocimetry technique for velocity and temperature fields *Exp. Fluids* **29** s129–40

Hu H and Koochesfahani M M 2003 A novel technique for quantitative temperature mapping in liquid by measuring the lifetime of laser induced phosphorescence *J. Vis.* **6** 143–53

Hu H, Lum C and Koochesfahani M M 2006 Molecular tagging thermometry with adjustable temperature sensitivity *Exp. Fluids* DOI:10.1007/s00348-006-0112-2

Koochesfahani M M 1999 Molecular tagging velocimetry (MTV): progress and applications *AIAA Paper No. AIAA-99-3786*

Koochesfahani M M (ed) 2000 Special feature: molecular tagging velocimetry *Meas. Sci. Technol.* **11** 1235–300

Koochesfahani M M, Cohn R K, Gendrich C P and Nocera D G 1996 Molecular tagging diagnostics for the study of kinematics and mixing in liquid phase flows *Proc. 8th Int. Symp. on Applications of Laser Techniques to Fluids Mechanics (Lisbon, Portugal, 8–11 July 1996)* vol I pp 1.2.1–1.2.12; also in: 1997 *Developments in Laser Techniques and Fluid Mechanics* ed R J Adrian *et al* (Berlin: Springer) chapter 2, section 1, p 125

Koochesfahani M M, Cohn R K and Mackinnon C G 2000 Simultaneous whole-field measurements of velocity and concentration fields using combined MTV and LIF *Meas. Sci. Technol.* **11** 1289–300

Kotsovinos N E 1977 Plane turbulent buoyant jets *J. Fluid Mech.* **81** 45–92

Lavielle P, Lemoine F, Lavergne G and Lebouche M 2001 Evaporating and combusting droplet temperature measurements using two-color laser-induced fluorescence *Exp. Fluids* **31** 45–55

Lemoine L, Antonie Y, Wolff M and Lebouche M 1999 Simultaneous temperature and 2D velocity measurements in a turbulent heated jet using combined laser-induced fluorescence and LDA *Exp. Fluids* **26** 315–23

Lempert W R and Harris S R 2000 Molecular tagging velocimetry *Flow Visualization—Techniques and Examples* ed A J Smits and T T Lim (London: Imperial College Press) pp 73–92

Mortellaro M A and Nocera D G 1996 A turn-on for optical sensing *Chem. Technol.* **26** 17–23

Park H G, Dabiri D and Gharib M 2001 Digital particle image velocimetry/thermometry and application to the wake of a heated circular cylinder *Exp. Fluids* **30** 327–38

Ponce A, Wong P A, Way J J and Nocera D G 1993 Intense phosphorescence trigged by alcohol upon formation of a cyclodextrin ternary complex *J. Phys. Chem.* **97** 11137–42

Pringsheim P 1949 *Fluorescence and Phosphorescence* (New York: Interscience)

Sakakibara J and Adrian R J 1999 Whole field measurement of temperature in water using two-color laser induced fluorescence *Exp. Fluids* **26** 7–15

Sakakibara J, Hishida K and Maeda M 1997 Vortex structure and heat transfer in the stagnation region of an impinging plane jet *Int. J. Heat Mass Transfer* **40** 3163–76

Thompson S L and Maynes D 2001 Spatially resolved temperature measurement in a liquid using laser induced phosphorescence *J. Fluid Eng.* **123** 293–302

Turro N J 1978 *Modern Molecular Photochemistry* (Menlo Park, CA: Benjamin-Cummings)